Local Air–Sea Relationship in Observations and Model Simulations

RENGUANG WU

Center for Ocean–Land–Atmosphere Studies, Calverton, Maryland

BEN P. KIRTMAN

School for Computational Sciences, George Mason University, Fairfax, Virginia, and Center for Ocean–Land–Atmosphere Studies, Calverton, Maryland

KATHY PEGION

School for Computational Sciences, George Mason University, Fairfax, Virginia

(Manuscript received 3 May 2005, in final form 21 December 2005)

ABSTRACT

The present study compares the local simultaneous correlation between rainfall–evaporation and sea surface temperature (SST)–SST tendency among observations, coupled general circulation model (CGCM) simulations, and stand-alone atmospheric general circulation model (AGCM) simulations. The purpose is to demonstrate to what extent the model simulations can reproduce the observed air–sea relationship. While the model-simulated correlation agrees with the observations in the tropical eastern Pacific, large discrepancies are found in the subtropics, midlatitudes, and tropical Indo-western Pacific Ocean regions. In tropical Indo-western Pacific Ocean regions and the midlatitudes where the atmosphere contributes to the observed SST changes, the specified SST simulations produce excessive SST forcing, whereas the CGCM captures the atmospheric feedback on the SST, but with somewhat of an overestimation. In the subtropics, both the AGCM and CGCM produce unrealistic positive rainfall–SST correlations. In the tropical western-central Pacific and the North Indian Ocean, the CGCM-simulated evaporation–SST correlation is opposite to that observed because of an excessive dependence of the sea–air humidity difference on the SST.

1. Introduction

Simulations of atmospheric general circulation models (AGCMs) with specified sea surface temperature (SST) forcing have been used to understand the importance of SST anomalies for atmospheric interannual variations (e.g., Shukla and Wallace 1983; Palmer et al. 1992; Kumar et al. 1994; Sperber and Palmer 1996; Trenberth et al. 1998; Kang et al. 2002; Wang et al. 2004). On the other hand, there is increasing evidence indicating that atmospheric changes contribute to SST anomalies in various regions (Bladé 1997; Barsugli and Battisti 1998; Lau and Nath 2000, 2003; Wang et al. 2000, 2003; Hendon 2003; Wu and Kirtman 2005). Can the specified SST simulation correctly reproduce the observed relationship between atmospheric variables and SST?

Fundamental discrepancies between the AGCM simulations and observations have been identified in previous studies (e.g., Palmer et al. 1992; Sperber and Palmer 1996; Kumar and Hoerling 1998; Kang et al. 2002; Wang et al. 2004). Large differences have also been found between AGCM and coupled general circulation model (CGCM) simulations, which have the same SST anomalies (Barsugli and Battisti 1998; Kitoh and Arakawa 1999; Lau and Nath 2000; Wu and Kirtman 2004, 2005). These studies indicate that the atmospheric models with prescribed SST forcing may produce large spurious surface heat fluxes in the midlatitudes (Barsugli and Battisti 1998), overestimate significantly the atmospheric variability in the North Indian Ocean and western North Pacific in boreal summer (Wu and Kirtman 2005), and misrepresent the relationship between the Indian summer monsoon and El Niño–Southern Oscillation (ENSO) (Wu and Kirtman 2004; Krishna Kumar et al. 2005; Wang et al. 2005).

Corresponding author address: Dr. Renguang Wu, Center for Ocean–Land–Atmosphere Studies, 4041 Powder Mill Road, Suite 302, Calverton, MD 20705.
E-mail: renguang@cola.iges.org

How the stand-alone AGCM simulations differ from the coupled simulations or observations depends on the character of the air–sea interaction. If the SST forcing of the atmosphere dominates, it is likely that the observed atmospheric variability can be captured by stand-alone AGCM simulations with specified SST forcing. This happens in the tropical central and eastern Pacific where AGCM simulations perform well (e.g., Wang et al. 2004). If the observed SST anomalies include significant atmospheric feedback, improper atmospheric changes could be induced in the specified SST simulations. This is the case in the North Pacific and tropical monsoon regions. AGCM simulations in these regions often have large discrepancies from observations (e.g., Wang et al. 2004; Wu and Kirtman 2005).

The nature of the local air–sea interaction can be characterized by the covariance or correlation between the atmospheric variables and SST (Frankignoul and Hasselmann 1977; Frankignoul 1985; Frankignoul et al. 1998; Barsugli and Battisti 1998; von Storch 2000). Using a simple stochastic model, Barsugli and Battisti (1998) identified a distinct lagged linear regression between sea and air temperatures for coupled and uncoupled cases. Frankignoul et al. (1998) showed that the cross correlation between heat flux and SST changes sign between negative and positive lags when the heat flux feedback is negative in a stochastic model. von Storch (2000) provided a conceptual interpretation of how the different shapes of lag cross correlations relate to different forcing-response relationships. The author identified very different evolution of the lag correlation between surface heat flux and SST in the midlatitude North Pacific and the equatorial central Pacific.

The objective of this study is to compare the local simultaneous correlation between rainfall–evaporation and SST–SST tendency among observations, CGCM simulations, and AGCM simulations on interannual time scales. This comparison is helpful for revealing not only the AGCM's potential problem, but also the CGCM's weakness in the simulation of the observed air–sea relationship. The rainfall is used in the analysis because it is a proxy for atmospheric heating in the Tropics. The surface evaporation is used because it is directly linked to the air–sea feedback both in the Tropics and midlatitudes. This study examines the relationship of both rainfall and surface evaporation with the SST and SST tendency. Note that the SST anomalies impact rainfall through both surface evaporation and SST gradient and thus the rainfall–SST correlation may differ from the evaporation–SST correlation. In the following, we first describe various datasets used in the present study (section 2). In section 3, we use a simple stochastic model to demonstrate that the local and simultaneous heat flux–SST and heat flux–SST tendency correlation is useful for distinguishing the atmospheric forcing of SST from the SST forcing of atmosphere. We compare the results of the correlation analysis derived from observations, CGCM simulations, and stand-alone AGCM simulations in section 4. The summary and discussions are provided in section 5.

2. Datasets

a. CMAP rainfall and Reynolds SST

The Climate Prediction Center (CPC) Merged Analysis of Precipitation (CMAP) (Xie and Arkin 1997) without the model input is used as a proxy for rainfall observations. The CMAP rainfall is on a 2.5° × 2.5° grid and is available starting from January 1979. The SST data are the Reynolds optimum interpolation SST analysis (Reynolds and Smith 1994) provided by the National Oceanic and Atmospheric Administration (NOAA)–Cooperative Institute for Research in Environmental Sciences (CIRES) Climate Diagnostics Center, obtained from their Web site (http://www.cdc.noaa.gov/). This SST dataset is on a 1° × 1° grid and covers the period from November 1981 to November 1998.

b. Satellite retrievals

Version 2 of the Goddard Satellite-Based Surface Turbulence Fluxes (GSSTF2) data provides the surface heat fluxes, which were obtained through an anonymous ftp (online at ftp://lake.nascom.nasa.gov/data/TRMM/Ancillary/gsstf). These surface heat fluxes are used as a proxy for observations in the present study. The GSSTF2 data are produced by the surface turbulent fluxes research group at the National Aeronautics and Space Administration (NASA) Goddard Space Flight Center (GSFC) (Chou et al. 2003). The variables include latent heat flux, sensible heat flux, zonal and meridional wind stress, surface air (~10 m) specific humidity, lowest-500-m precipitable water, 10-m wind speed, and the sea–air humidity difference. The data are on a 1° × 1° grid for the period of July 1987 through December 2000. The GSSTF2 turbulent fluxes are derived from the 10-m wind speed and 10-m specific humidity of version 4 Special Sensor Microwave Imager (SSM/I) products, as well as the 2-m air temperature and SSTs of the National Centers for Environmental Research–National Center for Atmospheric Research (NCEP–NCAR) reanalysis (Kalnay et al. 1996), using a bulk aerodynamic algorithm based on the surface layer similarity theory. Positive values of heat fluxes denote heat loss from the ocean.

The surface fluxes from the GSSTF2 dataset have biases due to errors in the parameterization of the flux model and uncertainties in the input variables (Chou et al. 2003). The bulk SST is used in the calculation of the saturation specific humidity at the sea surface with some approximations. The assumptions of von Kármán constants, errors in the parameterization of the flux model, and uncertainty in the input variables contribute to the flux errors. The GSSTF2 fluxes have been compared with other flux products (Chou et al. 2003, 2004; Curry et al. 2004). Comparison with observed fluxes of 10 field experiments suggests that the GSSTF2 heat fluxes are reasonable though there are regional biases (Chou et al. 2003).

c. Coupled model outputs

Outputs from two simulations of the CGCM at Center for Ocean–Land–Atmosphere Studies (COLA) are utilized in the analysis. The atmospheric component of the CGCM is the COLA global spectral AGCM with a horizontal resolution of T42 and 18 unevenly spaced vertical σ levels (Kinter et al. 1997). The oceanic component of the CGCM is version 3 of the Geophysical Fluid Dynamics Laboratory (GFDL) Modular Ocean Model (MOM3) (Pacanowski and Griffies 1998). For details of the CGCM, refer to Kirtman et al. (1997, 2002). The first CGCM simulation uses the conventional coupling method. The second CGCM simulation employs an anomaly coupling strategy (Kirtman et al. 1997, 2002). For convenience of distinguishing between the two simulations, the first one is called the fully coupled simulation (CGCM hereafter), and the second one is referred as the anomaly coupled simulation (ACGCM hereafter). The CGCM is integrated for 40 yr. The ACGCM simulation has multicentury outputs (Kirtman and Shukla 2002; Wu and Kirtman 2003; Yeh and Kirtman 2004). The ACGCM may be criticized because of the specification of its mean states. The CGCM may have climate drifts. The use of two versions of a coupled model in the present study is for the purpose of cross validating the coupled model results.

d. COLA AGCM simulations

Outputs from the COLA AGCM simulations with observed SST forcing are used in this diagnosis. These simulations are part of the Climate of the Twentieth Century (C20C) International Project (Kinter et al. 2004). The AGCM outputs cover the period of November 1948 through November 1998, with 10 ensemble members starting from different initial conditions. Similar integrations of the COLA AGCM with the SST forcing derived from the ACGCM simulation are also used in the present study. These model SST-forced simulations cover a 30-yr period. The initial conditions for these integrations were taken directly from the ACGCM simulation. These initial conditions were perturbed to obtain simulations deviating from the coupled model. Without these perturbations, the stand-alone AGCM simulations would reproduce the coupled model simulations as expected.

e. NCEP reanalysis version 2

We also use the NCEP–Department of Energy (DOE) reanalysis version 2 (Kanamitsu et al. 2002) outputs provided by the NOAA–CIRES Climate Diagnostics Center, obtained from their Web site online at http://www.cdc.noaa.gov/. The reanalysis variables are on a T62 grid and are available starting from January of 1979.

3. A simple stochastic model with white noise forcing

In this section, we use a simple stochastic model to demonstrate that the relative magnitude of local simultaneous correlations between heat flux and SST and between heat flux and SST tendency can provide guidance regarding the importance of atmospheric forcing versus SST forcing. Also, we show how the use of monthly means versus daily means affects the above correlation. Before presenting results of the stochastic model, in the following we first review the current literature regarding the use of local correlation in documenting air–sea feedbacks and discuss the strengths and weaknesses of various approaches.

a. Reviews of the use of local correlation

We first consider the simultaneous atmosphere–SST correlation. For given positive SST anomalies, rainfall often increases quickly through enhanced surface evaporation and low-level moisture convergence because of the relatively fast (1–2 weeks) atmospheric response to SST anomalies. This induces a positive simultaneous correlation between monthly mean rainfall and SST, which is typical of the tropical central and eastern Pacific (Trenberth and Shea 2005; Wang et al. 2005). Thus, a large positive simultaneous correlation, for example, between rainfall and SST, may indicate that the SST forcing of atmosphere dominates. However, the SST is also capable of responding to atmospheric forcing on time scales of days in some cases (Wallace et al. 1990). When the monthly means are

used, the simultaneous correlation between atmospheric variable and SST may include the atmospheric forcing of ocean (Wallace et al. 1990). In addition, the simultaneous correlation calculated based on monthly means may be impacted by atmospheric persistence (Frankignoul and Hasselmann 1977; Frankignoul et al. 1998). In such cases, it is difficult to determine, solely based on the above simultaneous correlation, whether the SST is forcing the atmosphere, the atmosphere is forcing the SST, or both fields are being forced by some other processes (Cayan 1992).

Because of the above reason, the lag–lead correlation needs to be examined to demonstrate how the atmosphere and ocean interact. As demonstrated by Barsugli and Battisti (1998) and von Storch (2000), the lag–lead correlation displays different evolution depending on the relative roles of atmospheric forcing and SST forcing. Analysis of lag–lead correlations had been used to estimate the intensity of heat flux feedbacks in observations and models (Frankignoul et al. 1998; von Storch 2000; Frankignoul and Kestenare 2002; Frankignoul et al. 2002; Frankignoul et al. 2004), and to examine the atmosphere–SST relationship and compare this relationship among observations, coupled model simulations, and AGCM simulations (Kitoh and Arakawa 1999; Arakawa and Kitoh 2004; Wang et al. 2005; Wu and Kirtman 2005). However, because atmosphere–ocean interactions are spatially and seasonally dependent, it is a rather time consuming process to analyze the lag–lead correlations for different regions.

Another way to avoid the ambiguity of simultaneous atmosphere–SST correlation is to relate the heat flux anomalies to the SST tendency (Cayan 1992). This is because the direct influence of the atmosphere on the ocean can be detected in the SST tendency. The simultaneous atmosphere–SST tendency correlation can indicate the change of the atmosphere–SST correlation across lag zero, and thus the atmospheric feedback on the ocean. For example, the coupled pattern of SST tendency and 500-hPa height is similar to that of SST and lag +2 week 500-hPa height both in the North Atlantic and the North Pacific (Deser and Timlin 1997). Wallace et al. (1990) pointed out that the interpretation of the corresponding pattern between atmospheric variables and the SST tendency is more straightforward compared to the pattern between atmosphere and SST itself. Analysis of the heat flux–SST tendency correlation has been performed to identify the atmospheric-forcing SST scenario in the North Pacific (Cayan 1992) and in the monsoon regions (Wu and Kirtman 2005). The value of the heat flux–SST tendency correlation also includes information about the contribution of other terms in the surface heat budget.

The literature cited above suggests that a combination of the simultaneous correlation of atmosphere–SST and atmosphere–SST tendency is useful for revealing whether SST anomalies force atmospheric changes or whether atmospheric changes contribute to SST anomalies. For example, Wu and Kirtman (2005) showed that in regions where the atmosphere has a strong feedback on SST [e.g., tropical western North Pacific in June–August (JJAS) and tropical southwestern Indian Ocean in December–February (DJF)], the simultaneous rainfall–SST tendency correlation is larger than the simultaneous rainfall–SST correlation in coupled model simulations. This differs from the equatorial central and eastern Pacific where the simultaneous rainfall–SST correlation is much larger than the simultaneous rainfall–SST tendency correlation.

b. Atmosphere forcing ocean

In this subsection, we use a simple stochastic model driven by white noise forcing to demonstrate that the relative importance of atmospheric forcing and SST forcing can be detected in the magnitude of simultaneous heat flux–SST and heat flux–SST tendency correlation. We first consider the case of atmospheric white noise forcing. The stochastic model used in the present study is a simplified version of that in Barsugli and Battisti (1998),

$$\frac{dT_a}{dt} = \alpha(T_o - T_a) + N_a, \tag{1}$$

$$\frac{dT_o}{dt} = \beta(T_a - T_o) - \gamma_o T_o. \tag{2}$$

In the above formula, T_a and T_o refer to air and sea temperature, respectively. Turbulent surface heat flux is represented using the sea–air temperature difference $(T_o - T_a)$. The N_a denotes the atmospheric Gaussian white noise forcing; γ_o is the radiation damping coefficient for T_o. The radiation damping for T_a is not considered in the present study. Note that the latent heat flux, which is proportional to the sea–air humidity difference, is linearly represented using the sea–air temperature difference. The value of parameters α and β depends on both the wind speed and the heat flux exchange coefficient. The exchange coefficient increases with the wind speed and increases inversely with the stability. The limitations of the above stochastic model were discussed in Barsugli and Battisti (1998).

The evolution of lag–lead correlation of the heat flux $(T_o - T_a)$ with the T_o and T_o tendency obtained from the stochastic model is shown in Fig. 1. In the integra-

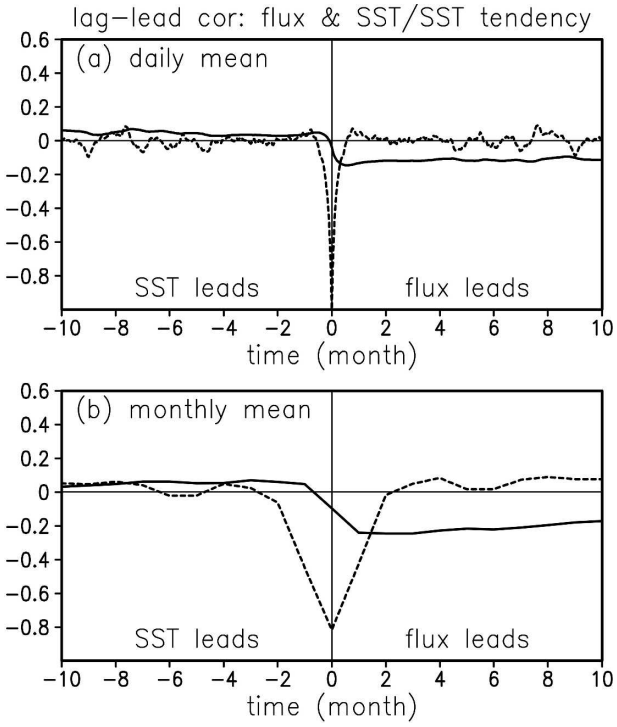

FIG. 1. Lag–lead correlation of turbulent heat flux–SST (solid curves) and turbulent heat flux–SST tendency (dashed curves) derived from a simple stochastic model with atmospheric white noise forcing. The correlation is calculated based on (a) daily and (b) monthly means.

tion of the stochastic model, the value for α is 23.9×10^{-7} s^{-1} and for γ_o is $1.9/2.0 \times 10^{-8}$ s^{-1}, following Barsugli and Battisti (1998), and the value for β is set to $\alpha/20$. The tendency is calculated based on centered differencing. The upper panel in Fig. 1 is the correlation calculated based on daily means, and the lower panel is the correlation calculated based on monthly means. The difference between the upper and lower panels indicates the smoothing effects resulting from the use of monthly means. Such smoothing effects were discussed by Frankignoul et al. (1998) who pointed out that the smoothing associated with the use of monthly averages generally increases the correlation at lags of plus and minus one in the case when there is negative atmospheric feedback (see their Fig. 2). A temporal resolution finer than 1 month is needed to obtain a more definite lag correlation structure (Deser and Timlin 1997).

From Fig. 1a, the heat flux–SST correlation is weakly positive when the SST leads and is negative when the heat flux leads. A quick decrease of the correlation occurs at lag 0. The correlation evolution in Fig. 1a is similar to that of Frankignoul et al. (1998) for the negative atmospheric feedback case (their Fig. 2, note that a different convention for the heat flux was used). This scenario indicates that the heat flux induced by positive SST anomalies feeds back negatively on SST. This atmospheric forcing of SST is clearly indicated by the large negative simultaneous heat flux–SST tendency correlation. In comparison, the simultaneous correlation between the heat flux and SST tendency is much larger than that between the heat flux and SST.

When the monthly means are used to calculate the correlation, the transition of the heat flux–SST correlation across lag 0 is less abrupt. The negative heat flux–SST tendency correlation not only appears at lag 0, but also at lags and leads of 1 month. In addition, the negative correlation at lag 0 is weaker. Nevertheless, the heat flux–SST tendency correlation at lag 0 is much larger than the corresponding heat flux–SST correlation, in agreement with the results from daily means.

The parameter values selected in the above stochastic model integrations are representative of those in the midlatitude North Pacific. Here, we apply this stochastic model to atmospheric white noise forcing in the Tropics. Our purpose is to mimic the observed lag–lead correlation in the equatorial central Pacific, which will be described later. For this purpose, we adjust values for the parameters in the stochastic model. We reduce β by 1/2 considering the effects of the mean wind speed decrease from midlatitudes to the Tropics, both directly through the wind speed itself and indirectly through reducing the exchange coefficient. We increase γ_o by a factor of 5 because the radiation effects are comparable to those of surface evaporation in the Tropics. The value for α is reduced by 1/20. This adjustment not only considers the effects of wind speed change, but also more importantly takes into account the fact that in the Tropics the surface air temperature displays large interannual variations, following closely those of SST. The changes in these parameter values are not intended to be quantitatively rigorous. Our purpose here is to provide a framework for interpreting the observational estimates and the CGCM results. While there is some sensitivity to the parameters, the qualitative comparisons presented remain valid for a wide range of parameter values.

The evolution of the lag–lead correlation calculated based on monthly means of the stochastic model simulation with adjusted parameter values is shown in Fig. 2a. From Fig. 2a, negative correlation appears at lag 0 for both the heat flux–SST and heat flux–SST tendency. The negative heat flux–SST correlation attains maximum when the heat flux leads SST by 1–3 months. The correlation evolution displays obvious asymmetry about lag 0. We will show later that the observed lag–

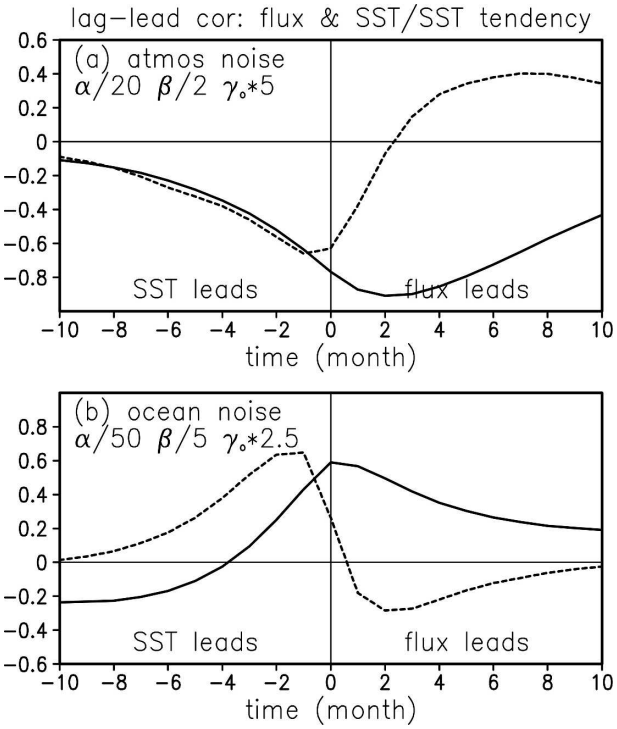

FIG. 2. Lag–lead correlation of turbulent heat flux–SST (solid curves) and turbulent heat flux–SST tendency (dashed curves) derived from a simple stochastic model with (a) atmospheric and (b) oceanic white noise forcing. The correlation is calculated based on monthly means. The adjustments for values of the parameters are indicated in the figures.

lead correlation evolution in the equatorial central Pacific qualitatively agrees with this simulated correlation evolution.

c. Ocean forcing atmosphere

The above stochastic model simulations are both driven by atmospheric white noise forcing. In the eastern equatorial Pacific, a high, positive simultaneous correlation is often observed between rainfall and SST (e.g., Trenberth and Shea 2005; Wang et al. 2005), and also between latent heat flux and SST (see Fig. 6a below). This positive correlation is indicative of SST forcing the atmosphere. Here, we show that a stochastic model with oceanic white noise forcing can capture the observed lag–lead correlation evolution. The stochastic model is as follows:

$$\frac{dT_a}{dt} = \alpha(T_o - T_a), \tag{3}$$

$$\frac{dT_o}{dt} = \beta(T_a - T_o) - \gamma_o T_o + N_o. \tag{4}$$

In the above formula, the N_o denotes the oceanic Gaussian white noise forcing. The meanings of the other parameters and variables are the same as in (1) and (2).

While the only change to the model equations was to remove the atmospheric stochastic forcing and introduce the oceanic stochastic forcing, the parameter values were changed. In particular, we reduce β by 1/5 of that used by Barsugli and Battisti (1998). This adjustment considers not only the effects of the wind speed reduction from the midlatitudes to the Tropics, but also the effects of enhanced stability in the eastern equatorial Pacific cold tongue region. Correspondingly, the value for α is reduced by 1/50 of that used by Barsugli and Battisti (1998). We increase γ_o by 2.5 times so that the radiation effect is on the same order as that of the surface evaporation.

The lag–lead correlation calculated based on monthly means of the above stochastic model simulation is shown in Fig. 2b. Large and positive heat flux–SST correlation appears at lag 0 and when heat flux leads SST by a few months. The simultaneous correlation between heat flux and SST tendency is much smaller than that between heat flux and SST. The large negative correlation between heat flux and SST tendency at lags and leads of several months is due to the smoothing effects. The heat flux–SST tendency correlation calculated based on daily means shows an abrupt change at lag 0, from weak positive to weak negative (not shown).

The results of stochastic model simulations demonstrate that a larger simultaneous heat flux–SST tendency correlation is indicative of atmosphere forcing SST, whereas a larger simultaneous heat flux–SST correlation is indicative of SST forcing the atmosphere. Thus, the magnitude of simultaneous heat flux–SST and heat flux–SST tendency correlations can be used to make inferences regarding the relative importance of atmospheric forcing and SST forcing.

Note, however, that this local perspective cannot account for the remote forcing. For example, the ENSO events can induce heat flux and SST changes in remote regions through atmospheric teleconnection (e.g., Lau and Nath 1996; Klein et al. 1999; Alexander et al. 2002). This may induce biases in the estimated local correlations (Frankignoul and Kestenare 2002; Frankignoul et al. 2004). The possible impacts of ENSO will be discussed in the last section. The local evaporation–SST correlation may be insufficient for describing a positive air–sea feedback arising from interaction of wind speed, evaporation, and SST (WES) in some climatic modes, such as the decadal tropical Atlantic SST mode (Chang et al. 1997; Xie and Tanimoto 1998).

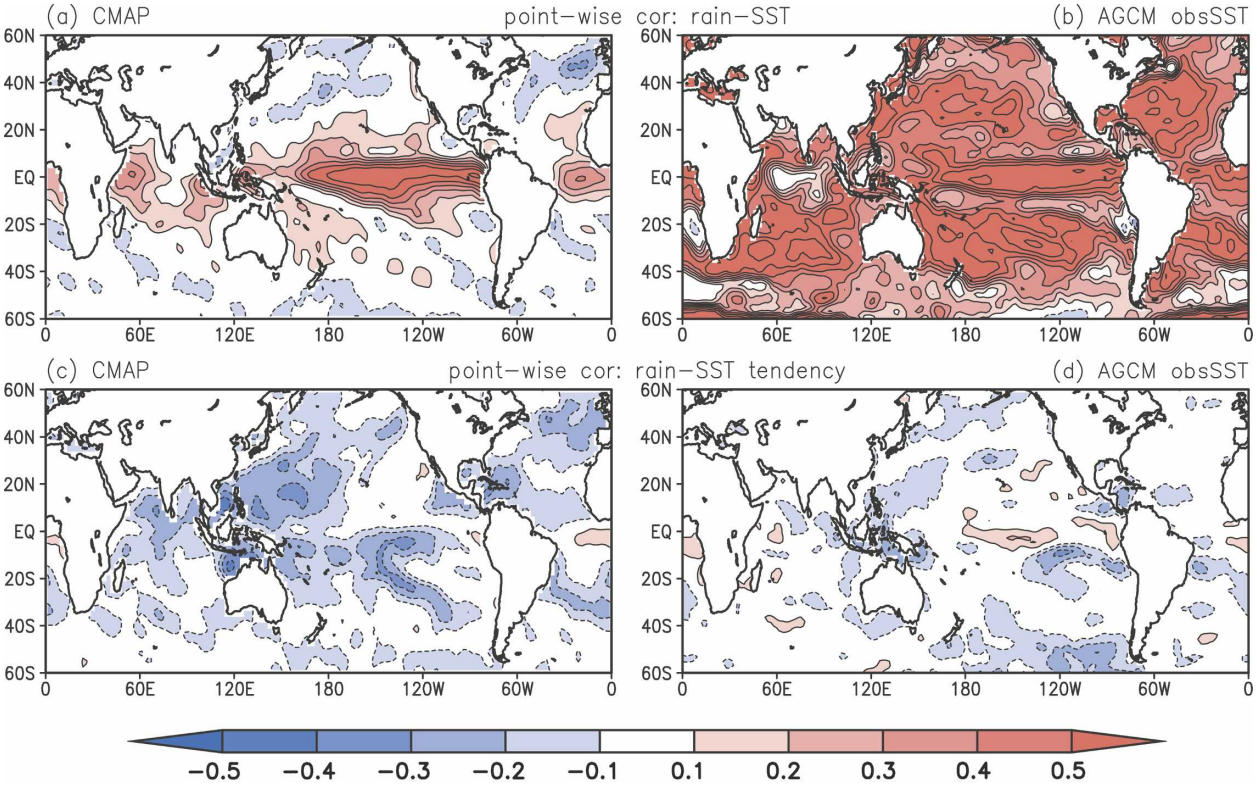

FIG. 3. Pointwise and simultaneous rainfall–SST correlation derived from (a) the CMAP and Reynolds SST and (b) the ensemble mean of 10 simulations of the COLA AGCM with observed SST forcing for the period from November 1981 to November 1998. (c), (d) Same as (a) and (b), except for rainfall–SST tendency correlation. The contour interval is 0.1 with zero contours suppressed.

4. Comparisons of correlation

In the following comparison between the observations and observed SST-forced AGCM simulations, the correlation coefficients were calculated over the same period. This excludes the potential impacts of using different time periods. Note that the differences between the observations and the coupled models may be affected by the bias of the coupled model means and the deviation of the model SST anomaly pattern from the observations. It should also be kept in mind that the observations have only one realization, whereas the correlation for the AGCM simulations are calculated based on the ensemble mean. The correlation shown for the model ensemble mean is generally higher than that for an individual member because of the noise reduction associated with ensemble averaging. The monthly mean SST tendency is calculated using centered differencing, that is, the difference of SST in the next month minus SST in the previous month. In the present study, the local correlations are calculated based on monthly means of all of the calendar months. The seasonal dependence of the air–sea relationship is not considered in this study, but will be investigated in the future.

a. Rainfall–SST and rainfall–SST tendency correlation

We start with comparing correlations between rainfall and SST because the rainfall–SST correlation is often discussed in the literature and rainfall is an important quantity as a proxy for atmospheric heating in the Tropics.

1) OBSERVATIONS VERSUS AGCM WITH THE OBSERVED SST FORCING

Figure 3 shows the rainfall–SST and rainfall–SST tendency correlation for the observations and the COLA AGCM simulations forced with the observed SST. Before calculating the correlation for the observations, the Reynolds SST was first interpolated to the CMAP rainfall grid. All of the correlations in Fig. 3 are based on the same period from November 1981 to November 1998.

Positive rainfall–SST correlation is seen in the tropical central-eastern Pacific and Atlantic Oceans, tropical western Indian Ocean, and tropical southeastern Indian Ocean near Sumatra, both in the AGCM simulations and in observations (Figs. 3a–b). The positive rainfall–SST correlation in the tropical eastern Pacific and west

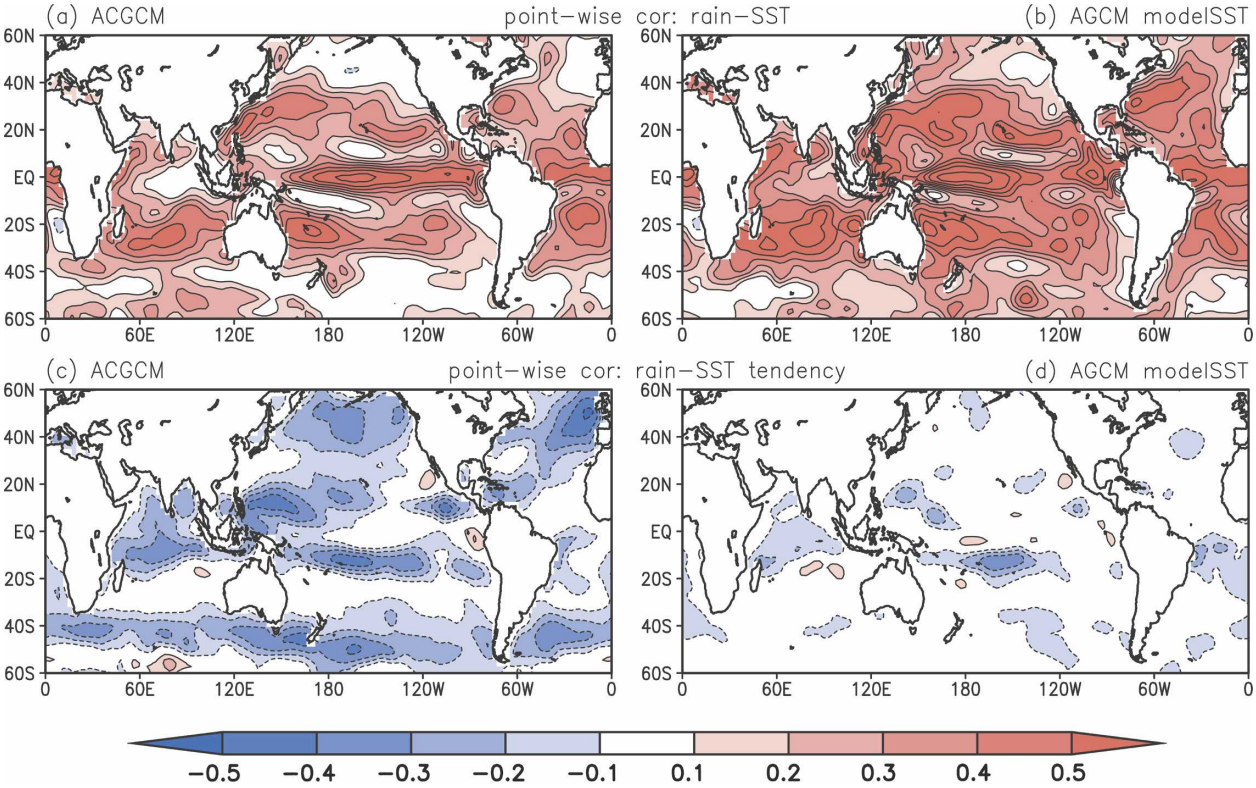

FIG. 4. Pointwise and simultaneous rainfall–SST correlation derived from (a) the COLA ACGCM 100-yr simulation and (b) the ensemble mean of ten 30-yr simulations of the COLA AGCM with the ACGCM-produced SST forcing. (c), (d) Same as (a) and (b), except for rainfall–SST tendency correlation. The contour interval is 0.1 with zero contours suppressed.

of Sumatra is due to a strong thermocline feedback in the generation of SST anomalies. Different rainfall–SST correlation appears in tropical northwestern Pacific and Atlantic Oceans, the Bay of Bengal, most of the subtropics, and the midlatitudes. In these regions, the rainfall–SST correlation is weak in the observations (Fig. 3a). In sharp contrast, large, positive correlation is seen in the AGCM simulations (Fig. 3b).

The rainfall–SST tendency correlation is very weak in the stand-alone AGCM simulations (Fig. 3d) because of the suppression of atmospheric-forced SST variability. In observations, moderate negative correlation is seen in the tropical northwestern Pacific and Atlantic Oceans, North Indian Ocean, and tropical South Pacific Ocean (Fig. 3c). This negative correlation indicates the atmospheric contribution to the observed SST change.

The CMAP rainfall has spurious decreasing trends over ocean, which is an artifact of input data and atoll sampling error (Yin et al. 2004). To demonstrate whether this will affect our results, we did parallel analysis with monthly rainfall from version 2 of the Global Precipitation Climatology Project (GPCP) (Adler et al. 2003). The obtained results are very similar to those based on CMAP rainfall.

2) COUPLED MODEL VERSUS AGCM WITH THE COUPLED MODEL SST FORCING

Now, we compare the rainfall–SST and rainfall–SST tendency correlation in the coupled model with the AGCM forced with prescribed SST taken from the coupled model simulation. The differences between the coupled model and the AGCM indicate the impacts of air–sea coupling because the coupled model uses the same AGCM. The time period for the correlation in the AGCM differs from that in the coupled model. This, however, does not affect our conclusions.

The rainfall–SST correlation in the Tropics is similar in the ACGCM and AGCM simulations (Figs. 4a–b). In comparison, the magnitude of positive correlation in tropical northwestern Pacific and Atlantic Oceans and the Bay of Bengal is higher in the stand-alone AGCM than in the ACGCM. In the midlatitudes, the stand-alone AGCM has a larger positive correlation compared to the ACGCM. The rainfall–SST correlation in the CGCM simulation (Fig. 5a) is similar to the

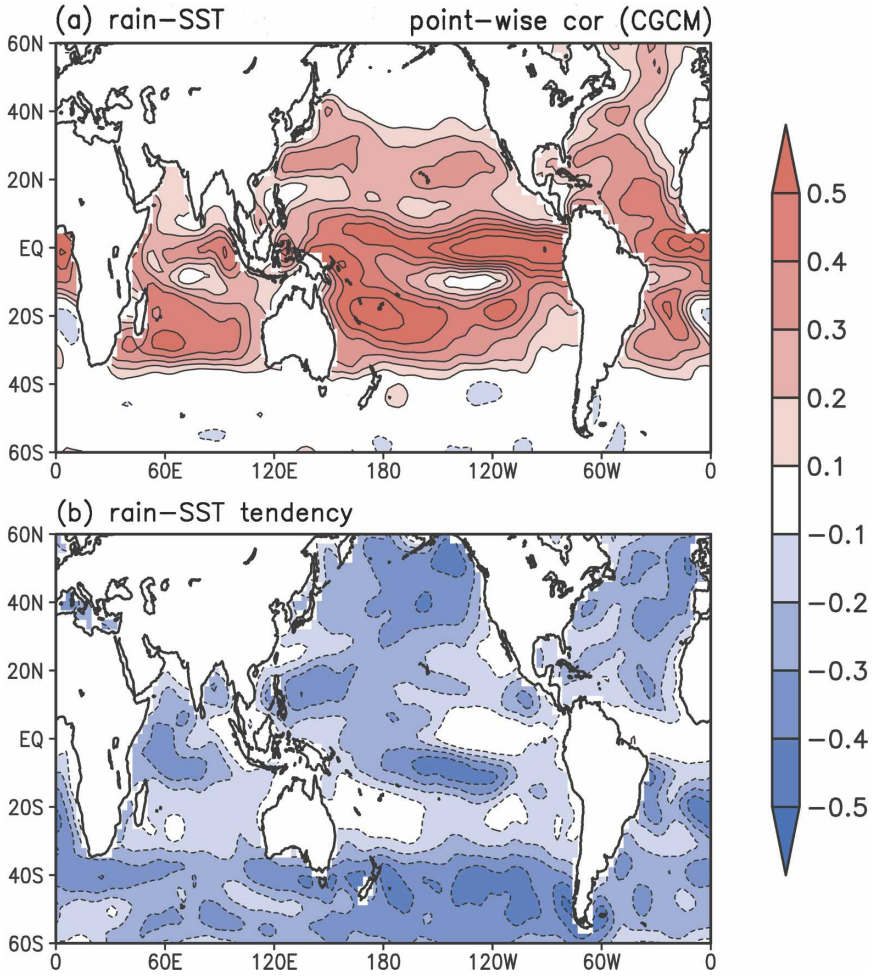

FIG. 5. Pointwise and simultaneous rainfall–SST correlation derived from (a) the COLA CGCM 40-yr simulation. (b) Same as (a), except for rainfall–SST tendency correlation. The contour interval is 0.1 with zero contours suppressed.

ACGCM in most regions. One noticeable difference is seen in the equatorial eastern Indian Ocean where a large, positive correlation appears in the CGCM (Fig. 5a) but not in the ACGCM (Fig. 4a). Another difference is that the positive correlation in the subtropical western North Pacific and the North Indian Ocean is weaker in the CGCM compared to the ACGCM.

The rainfall–SST tendency correlation is very weak in the stand-alone AGCM except for a small region in the tropical central South Pacific (Fig. 4d). In contrast, noticeable negative correlation is seen in the coupled models both in the Tropics and midlatitudes, including the tropical northwestern Pacific and Atlantic Ocean, tropical Indian Ocean, tropical South Pacific, midlatitude North Pacific and Atlantic Oceans, and midlatitudes of southern oceans (Figs. 4c, 5b). This indicates the contribution of atmospheric forcing in changing the SST in the coupled models.

One interesting feature in the coupled models is that negative rainfall–SST tendency correlation (Figs. 4c, 5b) often "fills the holes" of positive rainfall–SST correlation (Figs. 4a, 5a). This suggests that the atmospheric forcing and SST forcing are out of phase in space and that each of them has preferred locations. The reason for this is unknown.

3) OBSERVATIONS VERSUS COUPLED MODEL

The ACGCM captures the observed rainfall–SST correlation in most tropical regions (Fig. 4a versus Fig. 3a). Large discrepancies are seen in the subtropics, tropical northwestern Pacific and Atlantic Oceans, and North Indian Ocean. In these regions, the coupled model displays a large, positive rainfall–SST correlation (Fig. 4a). The CGCM (Fig. 5a) performs better than the ACGCM (Fig. 4a) in the North Indian Ocean, tropical western North Pacific, and tropical southeastern Indian

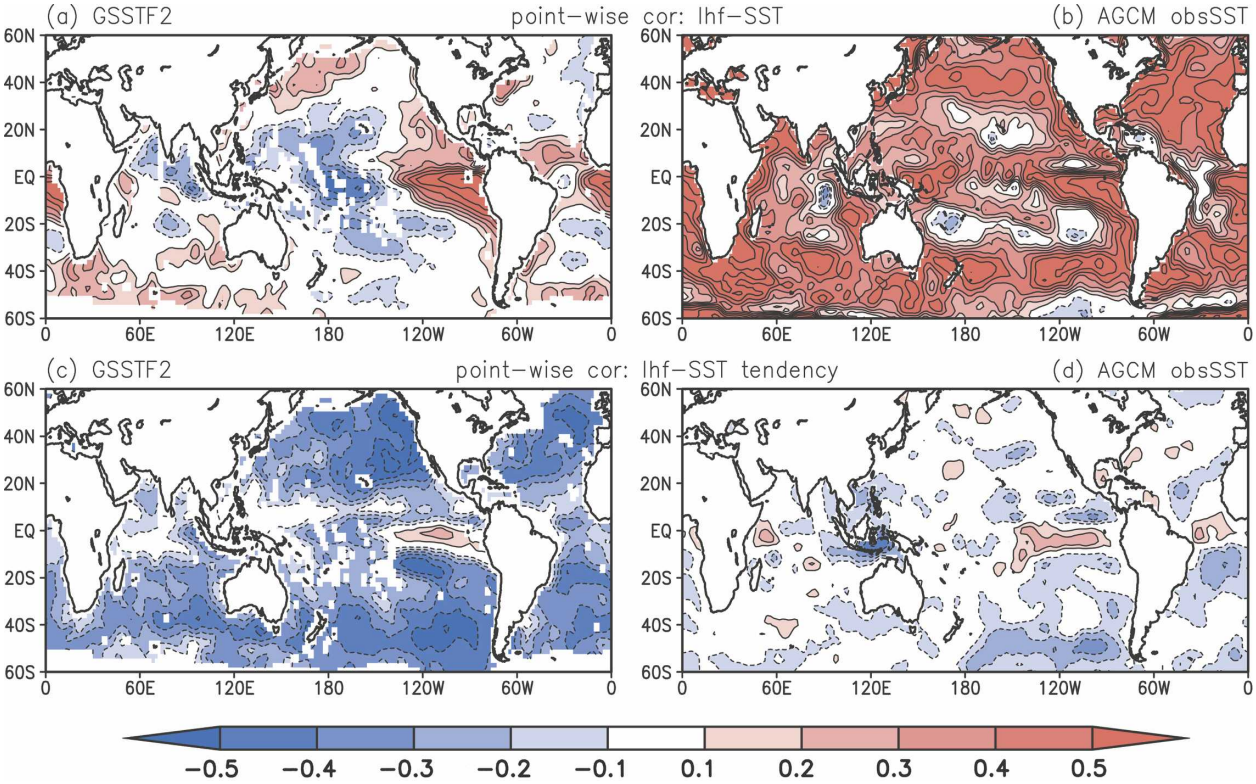

FIG. 6. Pointwise and simultaneous evaporation–SST correlation derived from (a) the GSSTF version 2 and (b) the ensemble mean of 10 simulations of the COLA AGCM with observed SST forcing for the period from January 1988 to November 1998. (c), (d) Same as (a) and (b), except for evaporation–SST tendency correlation. The contour interval is 0.1 with zero contours suppressed.

Ocean. The ACGCM and CGCM maps for the rainfall–SST correlation are more similar to each other than to that observed. This indicates that the mere act of coupling atmosphere and ocean models does not necessarily reproduce the observed relationship. Note that large, positive rainfall–SST correlation in the subtropical regions is also seen in the AGCM (Figs. 3b, 4b). This suggests that the problem may be in the AGCM physics, not in the coupling. There is, however, no explicit dependence of the model's convective parameterization on SST. The reason for this discrepancy remains to be understood. It should be pointed out that in the extratropics satellite rainfall estimates suffer from errors. For example, infrared algorithms fail to detect rainfall associated with shallow atmospheric systems. Thus, the rainfall–SST correlation may have "observational" errors.

The coupled models simulate the observed negative rainfall–SST tendency correlation in most regions (Figs. 4c, 5b versus Fig. 3c), which is missing in the standalone AGCM simulations (Figs. 3d, 4d). This agreement suggests that the coupled models capture important aspects of how the atmospheric forcing impacts the SST. In comparison, the negative rainfall–SST tendency correlation in the midlatitudes is higher in the coupled models than in observations. The negative rainfall–SST tendency correlation in some tropical regions (the equatorial Indian Ocean, the South Pacific convergence zone) is also somewhat higher in the coupled models compared to observations.

b. *Surface evaporation–SST and surface evaporation–SST tendency correlation*

1) OBSERVATIONS VERSUS AGCM WITH THE OBSERVED SST FORCING

This subsection examines the evaporation–SST and evaporation–SST tendency correlation. Figure 6 shows the correlation of the latent heat flux with SST and SST tendency derived from the GSSTF2 dataset and the AGCM simulations forced with the observed SST. These correlations were calculated for a 12-yr period from January 1988 to November 1998.

Large, positive evaporation–SST correlation is seen in the tropical eastern Pacific and Atlantic Oceans in both the observations and the AGCM simulations (Figs. 6a–b). The correlation in the tropical western-central Pacific and tropical North Indian Ocean are

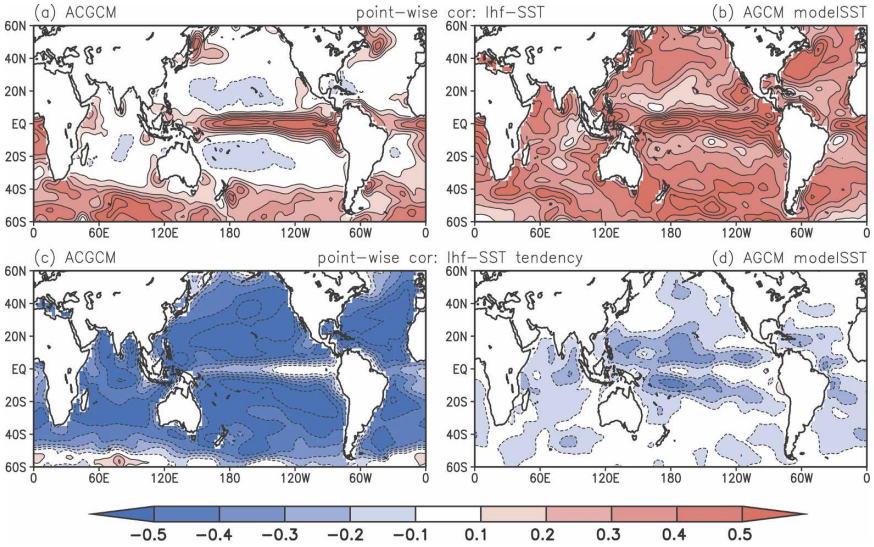

FIG. 7. The same as Fig. 4, except for (a), (b) evaporation–SST and (c), (d) evaporation–SST tendency correlations.

completely different—negative in the observations (Fig. 6a) but positive in the model (Fig. 6b). In the subtropics and midlatitudes, the AGCM is dominated by positive evaporation–SST correlation (Fig. 6b), whereas the observed evaporation–SST correlation is weak except for the western part of the North Pacific and Atlantic Oceans and some regions in the southern oceans (Fig. 6a). This indicates that the specified SST simulations may induce large spurious surface evaporation in the midlatitudes, consistent with Barsugli and Battisti (1998). This discrepancy may be, in part, due to the failure of the ensemble AGCM simulation in reproducing the observed wind variability and hence its correlation with SST in the extratropics.

The evaporation–SST tendency correlation is generally weak in the AGCM in both the Tropics and midlatitudes except for some localized regions (Fig. 6d). In the observations large, negative evaporation–SST tendency correlation is seen in the subtropics and midlatitudes (Fig. 6c), consistent with Cayan (1992), indicating a strong atmospheric forcing of SST changes. The negative correlation in the North Indian Ocean suggests the contribution of surface evaporation to SST anomalies, consistent with Lau and Nath (2000). Noticeable negative correlation is also seen along coastal Sumatra. In this region, surface evaporation contributes to SST anomalies (e.g., Wang et al. 2003; Hendon 2003; Lau and Nath 2004).

There are several discontinuities in surface evaporation of the GSSTF2 data resulting from the replacement of satellites (Chou et al. 2003). To examine the possible impacts of these discontinuities in satellite observations on our analysis, we calculated the correlation using subperiods of the GSSTF2 data within the same satellite observing period. The results do not show much difference.

2) COUPLED MODEL VERSUS AGCM WITH THE COUPLED MODEL SST FORCING

Positive evaporation–SST correlation appears in the equatorial Pacific and Atlantic Oceans and in the equatorial western Indian Ocean both in the ACGCM and AGCM (Figs. 7a–b). In comparison, the positive correlation in the North Indian Ocean and tropical northwestern Pacific is large in the stand-alone AGCM but very weak in the ACGCM. In the subtropics and northern midlatitudes, the stand-alone AGCM produces a high, positive correlation (Fig. 7b), which is barely seen in the ACGCM except for some small regions (Fig. 7a). The evaporation–SST correlation in the CGCM (Fig. 8a) generally agrees with the ACGCM (Fig. 7a). One exception is the equatorial eastern Indian Ocean where a large, positive correlation is seen in the CGCM (Fig. 8a) but not in the ACGCM (Fig. 7a).

The evaporation–SST tendency correlation is weak in the equatorial eastern Pacific and Atlantic Oceans both in the coupled models and the AGCM (Figs. 7c–d, 8b). In the tropical North and South Pacific and Atlantic Oceans, and the tropical Indian Ocean, the negative correlation is much stronger in the coupled models than in the AGCM. Pronounced discrepancies are seen in the subtropics and midlatitudes. In the coupled models large, negative correlation is present almost every-

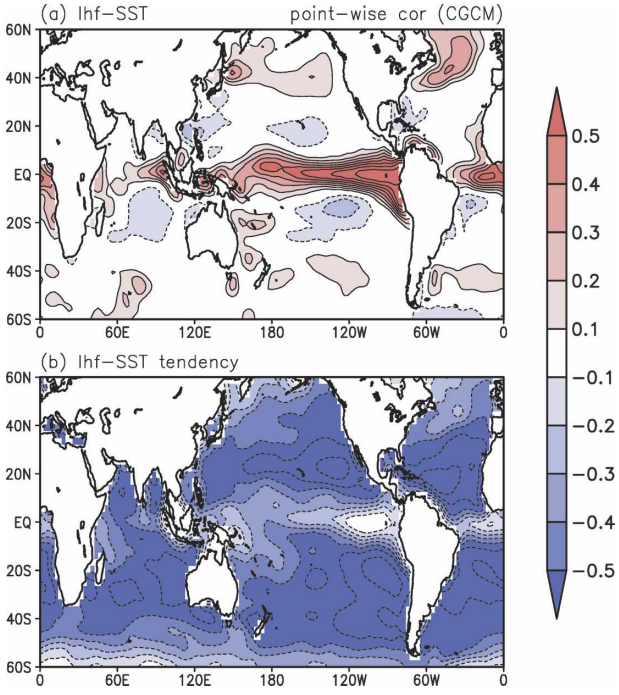

FIG. 8. The same as Fig. 5, except for (a), (b) evaporation–SST and (c), (d) evaporation–SST tendency correlations.

where (Figs. 7c, 8b), whereas in the AGCM the negative correlation is weak (Fig. 7d).

3) OBSERVATIONS VERSUS COUPLED MODEL

The coupled models cannot reproduce the negative evaporation–SST correlation in the North Indian Ocean and tropical western-central Pacific (Figs. 7a, 8a versus Fig. 6a). The discrepancy of evaporation–SST correlation in the western-central tropical Pacific is related to the bias in the model-simulated SST pattern associated with ENSO. In observations, during El Niño, the effect of increased SST on evaporation in the central Pacific is countered by that of the relaxed trade winds, whereas in the ACGCM El Niño's center of action shifts too far west, making the modeled central Pacific somewhat equivalent to the eastern Pacific in reality. In the northern midlatitudes, both coupled models generally agree with observations. In the southern midlatitudes, the evaporation–SST correlation is higher in the ACGCM (Fig. 7a) compared to the observations (Fig. 6a) and the CGCM (Fig. 8a).

Both coupled models capture the negative evaporation–SST tendency correlation in the subtropics and midlatitudes but with a general overestimation (Figs. 7c, 8b versus Fig. 6c). In the Tropics, the negative correlation in the coupled models seems too large compared to observations, especially in the tropical northwestern Pacific and tropical Indian Ocean.

4) LAG–LEAD CORRELATION OF AREA MEANS

To further demonstrate the differences in the air–sea relationship between observations and the model simulations, we compare the temporal evolution of lag–lead correlation calculated based on area means. We selected four regions. The first region is the central North Pacific where large, negative heat flux–SST tendency correlation is seen in observations and coupled model simulations, suggesting that the atmosphere is forcing the ocean. The second region is the eastern equatorial Pacific where high, positive heat flux–SST correlation is seen in all the cases, suggesting that the ocean is forcing the atmosphere. The other two regions are the central equatorial Pacific where all of the model simulations fail to capture the observed heat flux–SST relationship and the North Indian Ocean where the SST anomalies are closely related to the South Asian monsoon variability.

Figure 9 shows the lag–lead correlation of both latent heat flux–SST and latent heat flux–SST tendency for the central North Pacific region (35°–45°N, 170°E–150°W). In this region, the heat flux–SST correlation derived from observations is positive when the SST leads and switches to negative when the SST lags, with a quick change at lag 0 (Fig. 9a). The heat flux–SST tendency correlation fluctuates except for lag 0 at which a large, negative correlation appears. It is interesting to note that the above evolution of the lag–lead correlation looks very similar to that simulated by the simple stochastic model (Fig. 1b). This similarity suggests that the SST variations in the central North Pacific are primarily driven by atmospheric stochastic forcing. It also indicates that the local simultaneous correlation is useful for revealing the atmospheric forcing of SST.

The evolution of the lag–lead correlation based on the ACGCM simulation (Fig. 9c) resembles the observations. A similar evolution was identified in the ECHAM3–Large Scale Geostrophic Ocean General Circulation Model (LSG) coupled model (von Storch 2000, see her Fig. 15). This indicates that the coupled model can simulate the atmospheric forcing of SST in the central North Pacific region. In comparison, the negative heat flux–SST tendency correlation at lag 0 is somewhat larger than the observations. The standalone AGCM simulations, whether forced by observed or ACGCM-produced SST (Figs. 9b,d), display a different temporal evolution of the correlation. The heat flux–SST correlation at lag 0 is positive and large, whereas the negative heat flux–SST tendency correlation at lag 0 is much weaker compared to observations and the ACGCM simulation. The maximum negative correlation between the heat flux and SST tendency

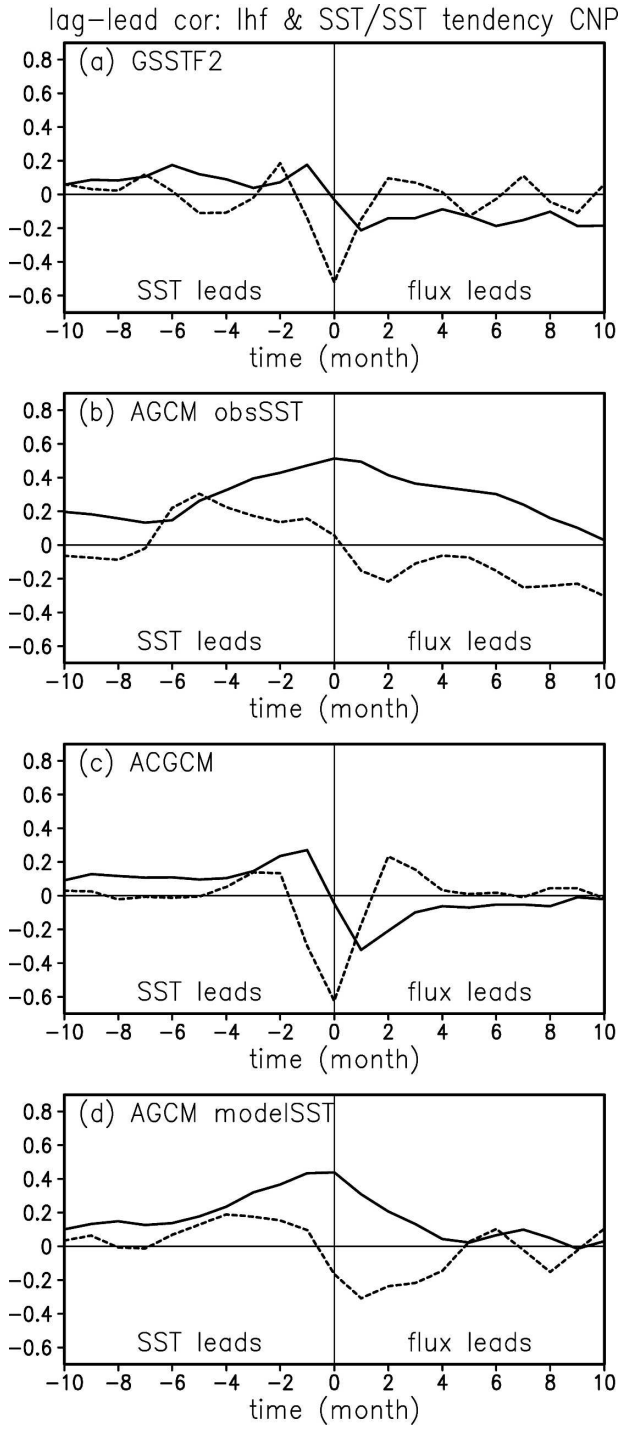

FIG. 9. Lag–lead correlation of latent heat flux–SST (solid curves) and latent heat flux–SST tendency (dashed curves) calculated based on area means in the central North Pacific region (35°–45°N, 170°E–150°W) derived from (a) the GSSTF version 2 for the period from January 1988 to November 1998, (b) the ensemble mean of 10 simulations of the COLA AGCM with observed SST forcing for the period from January 1988 to November 1998, (c) the COLA ACGCM 100-yr simulation, and (d) the ensemble mean of ten 30-yr simulations of the COLA AGCM with the ACGCM-produced SST forcing.

shifts to heat flux leading by 1–2 months. These discrepancies caution the use of AGCM simulations with specified SST forcing in the midlatitude North Pacific region.

Figure 10 is similar to Fig. 9 but for the eastern equatorial Pacific region (5°S–5°N, 130°–90°W). The evolution of lag–lead correlation in this region is distinct from that in the central North Pacific. In this region, the high and positive heat flux–SST correlation appears at lag 0 in observations (Fig. 10a). The heat flux–SST tendency correlation changes from positive, when SST leads, to negative, when SST lags. At lag 0, the heat flux–SST tendency correlation is much smaller than the heat flux–SST correlation. The above features are similar to that simulated by the stochastic model driven by oceanic white noise forcing (Fig. 2b). It is well known that in this region the SST forcing dominates. This suggests that a larger simultaneous heat flux–SST correlation compared to the simultaneous heat flux–SST tendency correlation is indicative of the dominance of SST forcing.

The evolution of observed lag–lead correlation is basically captured by the ACGCM (Fig. 10c). In comparison, the high, positive heat flux–SST correlation is maintained for a shorter time in the ACGCM compared to observations. This discrepancy could be due to the shorter ENSO period in the model (Kirtman et al. 2002). The stand-alone AGCM simulations (Figs. 10b,d) reproduce well the evolution of the observed or ACGCM-simulated correlation. This verifies the use of specified SST simulations in the eastern equatorial Pacific, which is in sharp contrast to the midlatitude North Pacific.

Figure 11 shows a lag–lead correlation similar to that in Fig. 9, but for the central equatorial Pacific region (5°S–5°N, 160°E–140°W). The observed correlation evolution (Fig. 11a) resembles that simulated by the stochastic model with atmospheric white noise forcing, though the magnitude of the correlation is smaller (Fig. 2a). This suggests that the atmospheric forcing may play an important role for SST anomalies in the central equatorial Pacific. Both ACGCM and stand-alone AGCM simulations display large and positive simultaneous heat flux–SST correlation and weak simultaneous heat flux–SST tendency correlation (Figs. 11b–d), which is indicative of SST forcing. This is pronouncedly different from the observations.

Figure 12 shows a correlation evolution similar to that in Fig. 8, but for the North Indian Ocean region (5°–20°N, 60°–100°E). The observed heat flux–SST correlation has noticeable negative correlation at lag 0 and +1 (Fig. 12a). The observed heat flux–SST tendency displays negative correlation at lags 0 and −1 and posi-

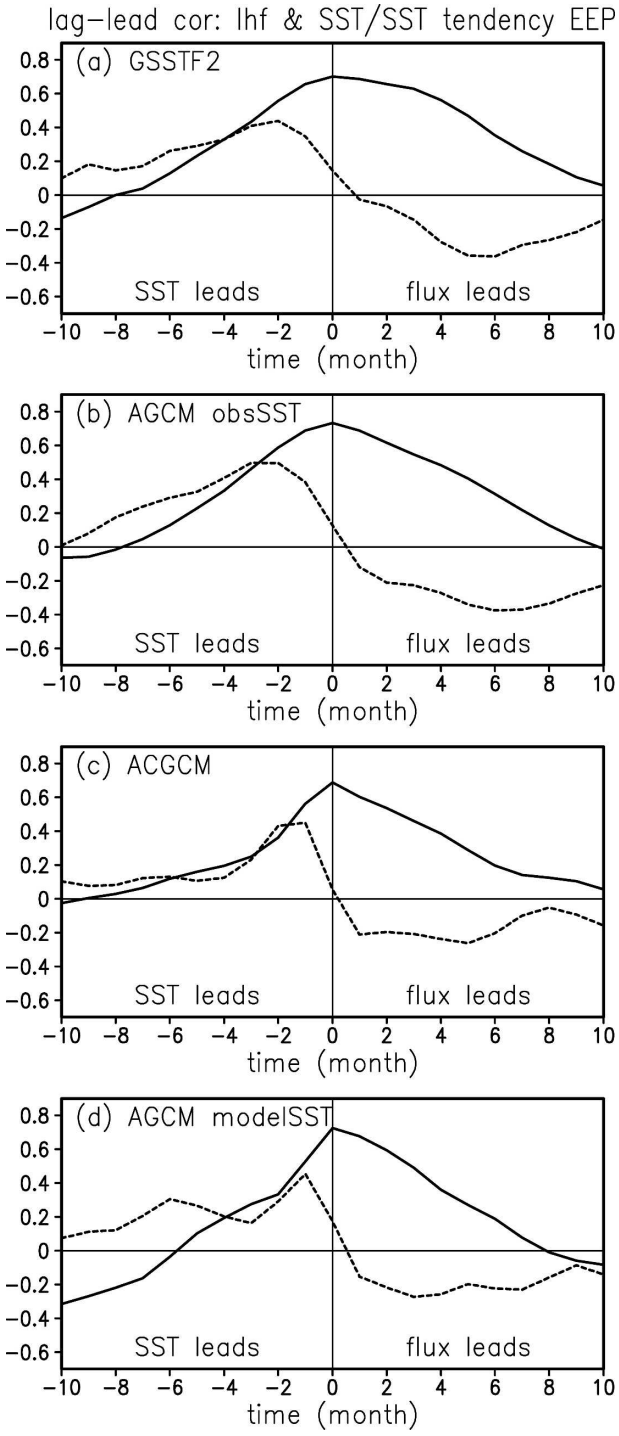

FIG. 10. The same as Fig. 9, except for area means in the eastern equatorial Pacific region (5°S–5°N, 130°W–90°).

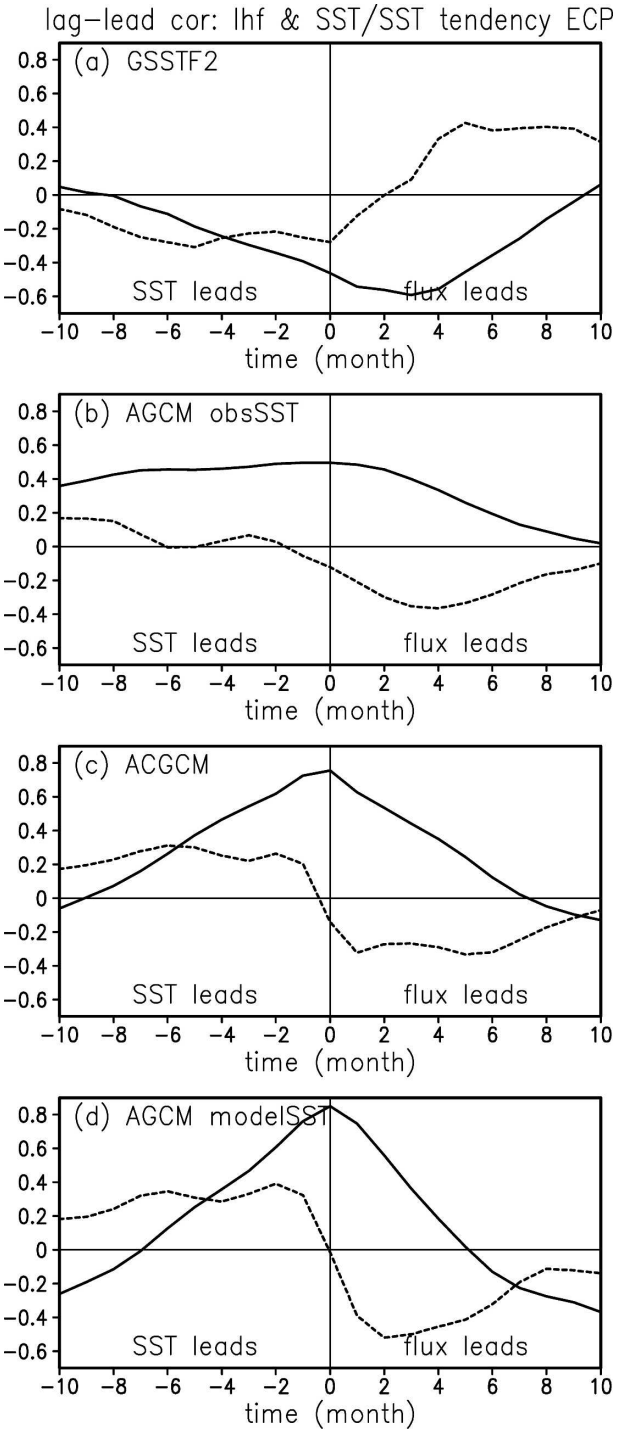

FIG. 11. The same as Fig. 9, except for area means in the central equatorial Pacific region (5°S–5°N, 160°E–140°W).

tive correlation around lag +2. The correlation evolution is similarity to that in Fig. 2a, suggesting the contribution of atmospheric forcing to SST anomalies. The ACGCM-simulated correlation evolution (Fig. 12c) resembles that in the central North Pacific, indicating the atmospheric forcing of SST. Compared to observations, the ACGCM overestimates the atmospheric forcing in the North Indian Ocean. Both observed and ACGCM

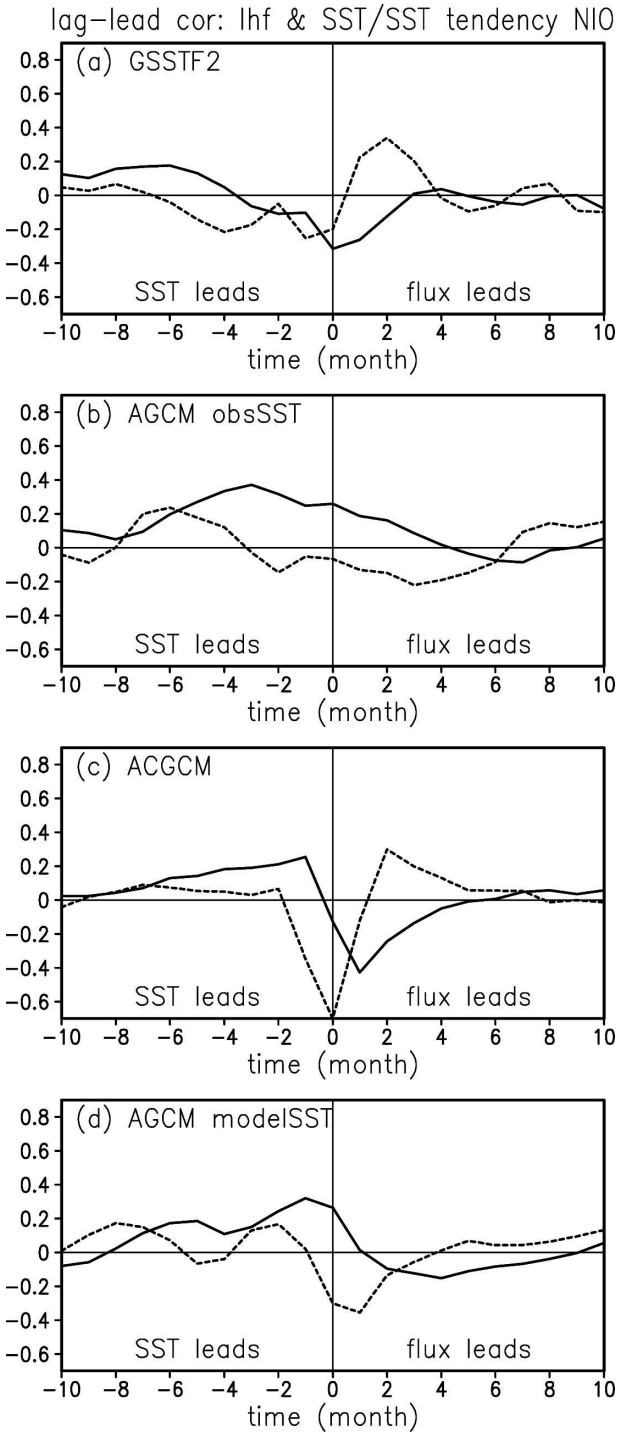

FIG. 12. The same as Fig. 9, except for area means in the North Indian Ocean region (5°–20°N, 60°–100°W).

SST-forced AGCM simulations display positive simultaneous heat flux–SST correlation (Figs. 12b,d), which is not seen in observations and ACGCM simulation. This suggests that specifying SST in this region would produce spurious surface evaporation.

c. *Contributions of wind speed–SST and sea–air humidity difference–SST correlation*

As pointed out above, the evaporation–SST correlation displays a pronounced discrepancy between the model simulations and observations in the North Indian Ocean and tropical western-central Pacific. We also noticed that the evaporation–SST correlation in the NCEP–DOE reanalysis differs considerably from observations in the above region. Figure 13 shows the evaporation–SST correlation derived from the reanalysis version 2. In Fig. 13, the correlation in the tropical western-central Pacific is generally weak with positive correlation in some localized regions. Positive correlation appears in the Arabian Sea, Bay of Bengal, South China Sea, and equatorial central-eastern Indian Ocean.

To understand the reason for the above discrepancy, we further examined the correlation between SST and surface wind speed, and that between SST and sea–air humidity difference. Note that the surface wind speed and sea–air humidity difference are two key components in calculating surface evaporation. Here, we show the correlation along the equatorial Indian and Pacific Oceans for observations, the ACGCM, and the reanalysis version 2 (Fig. 14). In estimating the correlation, the ACGCM wind speed is retrieved from surface wind stress components. The reanalysis monthly mean wind speed at 10 m is the average of daily mean wind speed derived from daily mean zonal and meridional wind components. The surface air humidity for observations and the reanalysis is at 10 and 2 m, respectively, whereas for the ACGCM we use the humidity at 1000 hPa (about 7–10 m in the equatorial western Pacific). This difference should not affect our comparisons.

In the equatorial eastern Pacific, the correlation between the air–sea humidity difference and SST is large and positive. In comparison, the correlation between the wind speed and SST is small. This is the case in the observations, ACGCM, and reanalysis. It is inferred that the positive evaporation–SST correlation in the equatorial eastern Pacific is mainly due to the sea–air humidity difference–SST correlation, which is consistent in the observations, coupled model, and reanalysis.

In the equatorial central Pacific, the observed negative evaporation–SST correlation is primarily contributed by the wind speed–SST correlation, which overcomes the positive sea–air humidity difference–SST correlation (Fig. 14a). In contrast, the positive evaporation–SST correlation in the coupled model is mainly due to the sea–air humidity difference–SST correlation (Fig. 14b). As a result, the surface evaporation anomalies are positive (negative) above positive (negative)

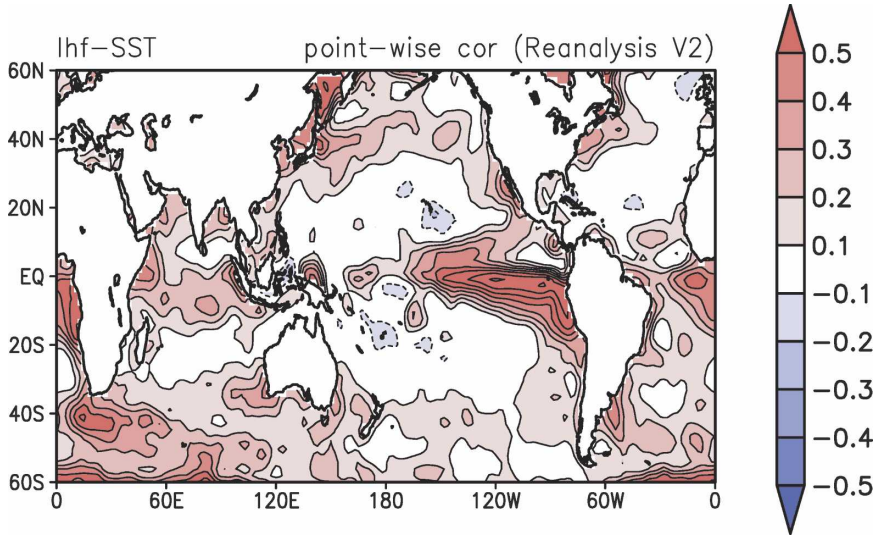

FIG. 13. Pointwise and simultaneous evaporation–SST correlation derived from the NCEP–DOE reanalysis version 2 for the period from January 1979 to December 2003. The contour interval is 0.1 with zero contours suppressed.

SST anomalies. In the reanalysis, the wind speed–SST correlation is quite large and negative and cancels most of the positive sea–air humidity difference–SST contribution (Fig. 14c). This leads to a weak correlation between the evaporation and SST. Note that in the equatorial western-central Pacific both the coupled model and the reanalysis have a much higher positive correlation between the sea–air humidity difference and SST compared to the observations. In the ACGCM, the wind speed–SST correlation is smaller compared to the observations and reanalysis. The excessive dependence of the sea–air humidity difference on SST in the coupled model and the reanalysis is also seen in the tropical Indian Ocean. Comparison of the surface air humidity–SST correlation indicates that in the tropical Indian Ocean–western Pacific, the surface air humidity anomalies closely follow the SST anomalies in observations, whereas in the coupled model the surface air humidity and SST anomalies are only weakly correlated. Further analysis is necessary to uncover the reason for the problem identified in the coupled model.

5. Summary and discussions

Using results from simple stochastic model simulations, we demonstrated that a combination of simultaneous heat flux–SST and heat flux–SST tendency correlations might indicate the relative importance of the atmospheric and SST forcing. Based on this, we compared the local correlation of rainfall–evaporation

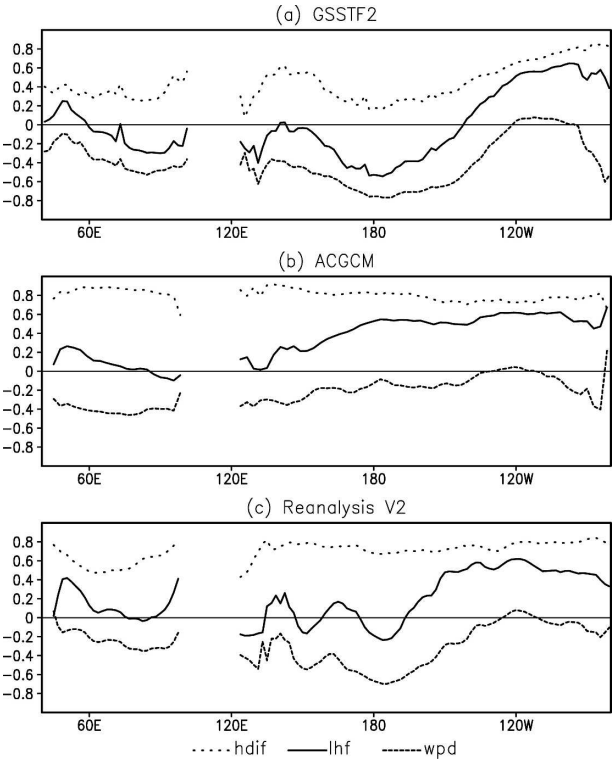

FIG. 14. Local and simultaneous correlation of surface evaporation (solid curves), sea–air humidity difference (dotted curves), and surface wind speed (dashed curves) with SST averaged over 5°S–5°N from (a) the GSSTF version 2 for the period of January 1988–December 2000, (b) the COLA ACGCM 100-yr simulation, (c) and the NCEP–DOE reanalysis version 2 for the period of January 1988–December 2000.

and SST–SST tendency in observations, stand-alone AGCM simulations, and coupled model simulations. Both consistencies and discrepancies are identified depending on geographical region.

The rainfall and SST correlation indicates that the COLA AGCM simulations produce excessive SST forcing of the atmosphere in the midlatitudes, subtropics, and tropical Indo-western Pacific Ocean regions. In these regions, based on observations, we conclude that the SST anomalies are significantly impacted by the atmospheric forcing, which the stand-alone AGCM simulations fail to capture. The COLA coupled model simulations produce excessive SST forcing of the atmosphere in the subtropics, and overestimate the SST forcing in the tropical Indo-western Pacific region and the atmospheric forcing of SST in the midlatitudes. The common failure of both the stand-alone AGCM and coupled model in simulating the rainfall–SST correlation in the subtropics points to problems in the atmospheric model physics.

Pronounced discrepancies from observations are found in the evaporation–SST correlation in the tropical Indian Ocean and western-central Pacific in both the coupled model and AGCM simulations. This weakness seems to be due to an excessive correlation between the sea–air humidity difference and SST in the models compared to observations. In the subtropics and midlatitudes, the AGCM produces spurious evaporation, whereas the coupled models capture the evaporation anomalies induced by the anomalous SST forcing. In the tropical Indo-Pacific region, the coupled models overestimate the role of surface evaporation for SST changes compared to the observations.

The comparison suggests that specifying SST forcing may produce excessive SST forcing in regions outside of the tropical eastern Pacific. The coupled models are able to produce some of the atmospheric forcing of the SST changes. Discrepancies, however, are still present. The reasons for these discrepancies may be multiple, including differing time scales, differing levels of noise, and differing atmospheric feedbacks. The bias in the coupled model means and the deviation of the model-simulated large-scale SST pattern from observations (such as those connected with ENSO) may contribute to these discrepancies. Further work is needed to determine the causes for the occurrence of these discrepancies. Similar analyses with other models would be necessary to understand the model dependence of the results.

While we caution the use of AGCM modeling using specified SSTs, there are cases in which the excessive local SST forcing of the atmosphere may not do too much damage. For example, in the midlatitudes, when SST anomalies contribute to low-frequency atmospheric variations, specification of the SST anomalies may add predictive skill to seasonal mean atmospheric states compared to not knowing SST anomalies, even though AGCM simulations generate spurious heat fluxes.

The local correlation does not consider the impacts of remote forcing. One such remote forcing is ENSO. To examine whether the ENSO forcing affects the local correlation, we recalculate the local correlation after removing the ENSO impacts using two different methods. In one method, we removed the ENSO impacts using linear simultaneous regression with respect to Niño-3.4 (5°S–5°N, 170°–120°W) SST anomalies. The correlation after removing the ENSO effects using this method does not show large changes in most regions away from the equatorial central and eastern Pacific. Note that the method of linear regression removes the instantaneous (on monthly time scale) linear effects of ENSO but not the possible delayed influence. Also, it neglects the nonlinearity of the ENSO teleconnections. In the other method, we recalculated the local correlation after excluding those months when the absolute value of the Niño-3.4 SST anomalies exceeds the 0.43 standard deviation. No significant changes have been identified, except for the equatorial Pacific. To confirm the above results, we computed the local correlation based on outputs from an ACGCM experiment in which climatological SSTs were specified in the Pacific Ocean. The obtained correlation in the Indian and Atlantic Oceans is similar to that calculated based on outputs from the control run for which the atmosphere and ocean are coupled in the Pacific Ocean. We conclude that the remote ENSO forcing does not affect the results of the present study, though further verification is necessary.

Acknowledgments. The authors appreciate comments of Jim Kinter, Kevin Trenberth, Dennis Shea, Bohua Huang, David Straus, and Sumant Nigam (editor). The thoughtful and constructive reviews of the two anonymous reviewers lead to significant improvement of this paper. This research was supported by grants from the National Science Foundation ATM-9814295 and ATM-0122859, the National Ocean and Atmospheric Administration NA16-GP2248, and the National Aeronautics and Space Administration NAG5-11656.

REFERENCES

Adler, R. F., and Coauthors, 2003: The version-2 Global Precipitation Climatology Project (GPCP) monthly precipitation analysis (1979–present). *J. Hydrometeor.,* **4,** 1147–1167.

Alexander, M. A., I. Bladé, M. Newman, J. R. Lanzante, N.-C. Lau, and J. D. Scott, 2002: The atmospheric bridge: The influence of ENSO teleconnections on air–sea interaction over the global oceans. *J. Climate,* **15,** 2205–2231.

Arakawa, O., and A. Kitoh, 2004: Comparison of local precipitation–SST relationship between the observation and a reanalysis dataset. *Geophys. Res. Lett.,* **31,** L12206, doi:10.1029/2004GL020283.

Barsugli, J. J., and D. S. Battisti, 1998: The basic effects of atmosphere–ocean thermal coupling on midlatitude variability. *J. Atmos. Sci.,* **55,** 477–493.

Bladé, I., 1997: The influence of midlatitude ocean–atmosphere coupling on the low-frequency variability of a GCM. Part I: No tropical SST forcing. *J. Climate,* **10,** 2087–2106.

Cayan, D. R., 1992: Latent and sensible heat flux anomalies over the northern oceans: Driving the sea surface temperature. *J. Phys. Oceanogr.,* **22,** 859–881.

Chang, P., L. Ji, and H. Li, 1997: A decadal climate variation in the tropical Atlantic Ocean from thermodynamic air-sea interactions. *Nature,* **385,** 516–518.

Chou, S.-H., E. Nelkin, J. Ardizzone, R. M. Atlas, and C.-L. Shie, 2003: Surface turbulent heat and momentum fluxes over global oceans based on Goddard satellite retrievals, version 2 (GSSTF2). *J. Climate,* **16,** 3256–3273.

——, ——, ——, and ——, 2004: A comparison of latent heat fluxes over global oceans for four flux products. *J. Climate,* **17,** 3973–3989.

Curry, J. A., and Coauthors, 2004: SEAFLUX. *Bull. Amer. Meteor. Soc.,* **85,** 409–424.

Deser, C., and M. S. Timlin, 1997: Atmosphere–ocean interaction on weekly timescales in the North Atlantic and Pacific. *J. Climate,* **10,** 393–408.

Frankignoul, C., 1985: Sea surface temperature anomalies, planetary waves, and air-sea feedbacks in the middle latitudes. *Rev. Geophys.,* **23,** 357–390.

——, and K. Hasselmann, 1977: Stochastic climate models. II: Application to sea-surface temperature anomalies. *Tellus,* **29,** 284–305.

——, and E. Kestenare, 2002: The surface heat flux feedback. Part I: Estimates from observations in the Atlantic and the North Pacific. *Climate Dyn.,* **19,** 633–647.

——, Z. Czaja, and B. L'Heveder, 1998: Air–sea feedback in the North Atlantic and surface boundary conditions for ocean models. *J. Climate,* **11,** 2310–2324.

——, E. Kestenare, and J. Mignot, 2002: The surface heat flux feedback. Part II: Direct and indirect estimates in the ECHAM4/OPA8 coupled GCM. *Climate Dyn.,* **21,** 27–51.

——, ——, M. Botzet, A. F. Carril, H. Drange, A. Pardaens, L. Terray, and R. Sutton, 2004: An intercomparison between the surface heat flux feedback in five coupled models, COADS and the NCEP reanalysis. *Climate Dyn.,* **22,** 373–388.

Hendon, H., 2003: Indonesia rainfall variability: Impacts of ENSO and local air–sea interaction. *J. Climate,* **16,** 1775–1790.

Kalnay, E., and Coauthors, 1996: The NCEP/NCAR 40-Year Reanalysis Project. *Bull. Amer. Meteor. Soc.,* **77,** 437–471.

Kanamitsu, M., W. Ebisuzaki, J. Woollen, S.-K. Yang, J. J. Hnilo, M. Fiorino, and G. L. Potterl, 2002: NCEP–DOE AMIP-II Reanalysis (R-2). *Bull. Amer. Meteor. Soc.,* **83,** 1631–1643.

Kang, I.-S., and Coauthors, 2002: Intercomparison of GCM simulated anomalies associated with the 1997/98 El Niño. *J. Climate,* **15,** 2791–2805.

Kinter, J. L., III, and Coauthors, 1997: The COLA atmosphere-biosphere general circulation model. Volume 1: Formulation. COLA Tech. Rep. 51, 46 pp.

——, M. J. Fennessy, V. Krishnamurthy, and L. Marx, 2004: An evaluation of the apparent interdecadal shift in the tropical divergent circulation in the NCEP–NCAR reanalysis. *J. Climate,* **17,** 349–361.

Kirtman, B. P., and J. Shukla, 2002: Interactive coupled ensemble: A new coupling strategy for CGCMs. *Geophys. Res. Lett.,* **29,** 1367, doi:10.1029/2002GL014834.

——, ——, B. Huang, Z. Zhu, and E. K. Schneider, 1997: Multiseasonal prediction with a coupled tropical ocean global atmosphere system. *Mon. Wea. Rev.,* **125,** 789–808.

——, Y. Fan, and E. K. Schneider, 2002: The COLA global coupled and anomaly coupled ocean–atmosphere GCM. *J. Climate,* **15,** 2301–2320.

Kitoh, A., and O. Arakawa, 1999: On overestimation of tropical precipitation by an atmospheric GCM with prescribed SST. *Geophys. Res. Lett.,* **26,** 2965–2968.

Klein, S. A., B. J. Soden, and N.-C. Lau, 1999: Remote sea surface temperature variations during ENSO: Evidence for a tropical atmospheric bridge. *J. Climate,* **12,** 917–932.

Krishna Kumar, K., M. Hoerling, and B. Rajagopalan, 2005: Advancing dynamical prediction of Indian monsoon rainfall. *Geophys. Res. Lett.,* **32,** L08704, doi:10.1029/2004GL021979.

Kumar, A., and M. P. Hoerling, 1998: Specification of regional sea surface temperatures in atmospheric general circulation model simulations. *J. Geophys. Res.,* **103,** 8901–8907.

——, A. Leetmaa, and M. Ji, 1994: Simulation of atmospheric variability induced by sea surface temperatures and implications for global warming. *Science,* **266,** 632–634.

Lau, N.-C., and M. J. Nath, 1996: The role of the "atmospheric bridge" in linking tropical Pacific ENSO events to extratropical SST anomalies. *J. Climate,* **9,** 2036–2057.

——, and ——, 2000: Impact of ENSO on the variability of the Asian–Australian monsoons as simulated in GCM experiments. *J. Climate,* **13,** 4287–4309.

——, and ——, 2003: Atmosphere–ocean variations in the Indo-Pacific sector during ENSO episodes. *J. Climate,* **16,** 3–20.

——, and ——, 2004: Coupled GCM simulation of atmosphere–ocean variability associated with zonally asymmetric SST changes in the tropical Indian Ocean. *J. Climate,* **17,** 245–265.

Pacanowski, R. C., and S. M. Griffies, 1998: MOM 3.0 manual. NOAA/GFDL, 638 pp.

Palmer, T. N., C. Brankovic, P. Viterbo, and M. J. Miller, 1992: Modeling interanual variations of summer monsoons. *J. Climate,* **5,** 399–417.

Reynolds, R. W., and T. Smith, 1994: Improved global sea surface temperature analysis using optimum interpolation. *J. Climate,* **7,** 929–948.

Shukla, J., and J. M. Wallace, 1983: Numerical simulation of the atmospheric response to equatorial sea surface temperature anomalies. *J. Atmos. Sci.,* **40,** 1613–1630.

Sperber, K. R., and T. N. Palmer, 1996: Interannual tropical rainfall variability in general circulation model simulations associated with the Atmospheric Model Intercomparison Project. *J. Climate,* **9,** 2727–2750.

Trenberth, K. E., and D. J. Shea, 2005: Relationships between precipitation and surface temperature. *Geophys. Res. Lett.,* **32,** L14703, doi:10.1029/2005GL022760.

——, G. W. Branstator, D. Karoly, A. Kumar, N.-C. Lau, and C. Ropelewski, 1998: Progress during TOGA in understanding and modeling global teleconnections associated with tropical

sea surface temperatures. *J. Geophys. Res.,* **103,** 14 291–14 324.

von Storch, J.-S., 2000: Signature of air–sea interactions in a coupled atmosphere–ocean GCM. *J. Climate,* **13,** 3361–3379.

Wallace, J. M., C. Smith, and Q.-R. Jiang, 1990: Spatial patterns of atmosphere-ocean interaction in the northern winter. *J. Climate,* **3,** 990–998.

Wang, B., R. Wu, and X. Fu, 2000: Pacific–East Asian teleconnection: How does ENSO affect East Asian climate? *J. Climate,* **13,** 1517–1536.

——, ——, and T. Li, 2003: Atmosphere–warm ocean interaction and its impacts on the Asian–Australian monsoon variation. *J. Climate,* **16,** 1195–1211.

——, I.-S. Kang, and J.-Y. Li, 2004: Ensemble simulation of Asian–Australian monsoon variability by 11 AGCMs. *J. Climate,* **17,** 803–818.

——, Q. Ding, X. Fu, I.-S. Kang, K. Jin, J. Shukla, and F. Doblas-Reyes, 2005: Fundamental challenge in simulation and prediction of summer monsoon rainfall. *Geophys. Res. Lett.,* **32,** L15711, doi:10.1029/2005Gl022734.

Wu, R., and B. P. Kirtman, 2003: On the impacts of the Indian summer monsoon on ENSO in a coupled GCM. *Quart. J. Roy. Meteor. Soc.,* **129,** 3439–3468.

——, and ——, 2004: Impacts of the Indian Ocean on the Indian summer monsoon–ENSO relationship. *J. Climate,* **17,** 3037–3054.

——, and ——, 2005: Roles of Indian and Pacific Ocean air–sea coupling in tropical atmospheric variability. *Climate Dyn.,* **25,** 155–170.

Xie, P., and P. A. Arkin, 1997: Global precipitation: A 17-year monthly analysis based on gauge observations, satellite estimates, and numerical model outputs. *Bull. Amer. Meteor. Soc.,* **78,** 2539–2558.

Xie, S.-P., and Y. Tanimoto, 1998: A pan-Atlantic decadal climate oscillation. *Geophys. Res. Lett.,* **25,** 2185–2188.

Yeh, S.-W., and B. P. Kirtman, 2004: The impact of internal atmospheric variability on North Pacific decadal variability. *Climate Dyn.,* **22,** 721–732.

Yin, X., A. Gruber, and P. Arkin, 2004: Comparison of the GPCP and CMAP merged gauge–satellite monthly precipitation products for the period 1979–2001. *J. Hydrometeor.,* **5,** 1207–1222.